AGU PUBLICATIONS

Paleoceanography

RESEARCH ARTICLE
10.1002/2014PA002774

Modeling oxygen isotopes in the Pliocene: Large-scale features over the land and ocean

Julia C. Tindall[1] and Alan M. Haywood[1]

[1] School of Earth and Environment, University of Leeds, Leeds, UK

Key Points:
- Model simulations of Pliocene $\delta^{18}O_{sw}$ and $\delta^{18}O_p$ presented
- The $\delta^{18}O_{sw}$ is a good proxy for local Pliocene salinity
- Model results useful in quantitatively relating $\delta^{18}O_p$ to climate

Supporting Information:
- Readme
- Data Set S1

Correspondence to:
J. C. Tindall,
J.C.Tindall@leeds.ac.uk

Citation:
Tindall, J. C., and A. M. Haywood (2015), Modeling oxygen isotopes in the Pliocene: Large-scale features over the land and ocean, *Paleoceanography*, *30*, 1183–1201, doi:10.1002/2014PA002774.

Received 24 DEC 2014
Accepted 29 JUL 2015
Accepted article online 8 AUG 2015
Published online 20 SEP 2015

Abstract The first isotope-enabled general circulation model (GCM) simulations of the Pliocene are used to discuss the interpretation of $\delta^{18}O$ measurements for a warm climate. The model suggests that spatial patterns of Pliocene ocean surface $\delta^{18}O$ ($\delta^{18}O_{sw}$) were similar to those of the preindustrial period; however, Arctic and coastal regions were relatively depleted, while South Atlantic and Mediterranean regions were relatively enriched. Modeled $\delta^{18}O_{sw}$ anomalies are closely related to modeled salinity anomalies, which supports using $\delta^{18}O_{sw}$ as a paleosalinity proxy. Modeled Pliocene precipitation $\delta^{18}O$ ($\delta^{18}O_p$) was enriched relative to the preindustrial values (but with depletion of <2‰ over some tropical regions). While usually modest (<4‰), the enrichment can reach 25‰ over ice sheet regions. In the tropics $\delta^{18}O_p$ anomalies are related to precipitation amount anomalies, although there is usually a spatial offset between the two. This offset suggests that the location of precipitation change is more uncertain than the amplitude when interpreting $\delta^{18}O_p$. At high latitudes $\delta^{18}O_p$ anomalies relate to temperature anomalies; however, the relationship is neither linear nor spatially coincident: a large $\delta^{18}O_p$ signal does not always translate to a large temperature signal. These results suggest that isotope modeling can lead to enhanced synergy between climate models and climate proxy data. The model can relate proxy data to climate in a physically based way even when the relationship is complex and nonlocal. The $\delta^{18}O$-climate relationships, identified here from a GCM, could not be determined from transfer functions or simple models.

1. Introduction

The mid-Pliocene Warm Period (mPWP), which occurred between 3.264 and 3.025MaB.P., has been intensively studied. This period is conventionally viewed as having a warm and stable climate, where global annual mean sea surface temperatures were 2–3°C higher than preindustrial values [*Dowsett et al.*, 2010; *Haywood et al.*, 2000], the same as is predicted by the Intergovernmental Panel on Climate Change (IPCC) by the end of this century [*Stocker et al.*, 2013]. Global ice volume was reduced by up to one third with large fluctuations over Greenland and West Antarctica [*Dolan et al.*, 2011], and global sea level was ≈22m higher [*Miller et al.*, 2012]. Despite these differences, the mPWP represents a familiar world as it shares many features with the modern: the continental configuration, orography (outside the ice sheet regions), and ocean bathymetry are all similar to today's. By understanding the climate of the mPWP, we can understand how the climate system operates in a warmer world.

The mPWP has been the focus of the Pliocene Research Interpretations and Synoptic Mapping(PRISM) [*Dowsett et al.*, 1994] project and the Pliocene Model Intercomparison Project (PlioMIP) [*Haywood et al.*, 2010, 2011]. PRISM has synthesized geological data to provide global paleoenvironmental reconstructions of the mid-Pliocene, and the current version, PRISM3D, has been used to provide either boundary conditions or validation data sets for model simulations undertaken as part of PlioMIP [*Dowsett et al.*, 2013].

Although not included in the PRISM3 data set, there is a wealth of oxygen isotope data. These have been collected over several decades and include oxygen isotopes measured in ocean-dwelling foraminifera [e.g., *Wara et al.*, 2005; *Tian et al.*, 2002] and coral [*Watanabe et al.*, 2011]. Oxygen (O) isotope measurements are generally converted to a δ notation by referencing the ratio of the heavy to light isotope ($R = {}^{18}O/{}^{16}O$) against a standard as

$$\delta^{18}O = ((R_{sample}/R_{standard}) - R_{standard}) \times 1000. \quad (1)$$

Although widely available, there are difficulties in extracting climate signals from $\delta^{18}O$. The largest source of $\delta^{18}O$ observations of Pliocene age is provided by foraminifera. For foraminifera the $\delta^{18}O$ signal in the

calcite shell ($\delta^{18}O_c$) provides an imprint of the $\delta^{18}O$ of seawater ($\delta^{18}O_{sw}$) in which the foraminifera lived, which is modified by the temperature (T) of the seawater at the time. Hence, $\delta^{18}O_c$, in surface dwelling planktonic foraminifera, can be used to determine either paleosurface $\delta^{18}O_{sw}$ or paleosurface ocean temperature, according to equations such as

$$T = a - b(\delta^{18}O_c - \delta^{18}O_{sw}) + c(\delta^{18}O_c - \delta^{18}O_{sw})^2, \quad (2)$$

where a, b, and c depend on the species considered [*Bemis et al.*, 1998].

For a foraminifera test to faithfully record Pliocene conditions it must be exceptionally well preserved and not have been subject to diagenetic alteration. *Williams et al.* [2005] noted that $\delta^{18}O_c$ from a number of Pliocene foraminifera from the North Atlantic suggested cooler temperatures than those derived from Mg/Ca data or the HadCM3 climate model. Such a signal could have occurred if the data had been subject to diagenesis. For exceptionally well-preserved foraminifera, which have not been subjected to diagenesis, climate information can be derived from $\delta^{18}O_c$ providing the $\delta^{18}O_{sw}$, and the temperature signals can be disentangled, for example, by using paired Mg/Ca and $\delta^{18}O_c$ data from the same foraminifera test [e.g., *Karas et al.*, 2009]. In this way the temperature is estimated from the Mg/Ca data which is then used along with equation (2) to determine $\delta^{18}O_{sw}$; however, because this is a two-step process, measurement and calibration errors will be compounded and can become significant [*Rohling*, 2007]. When derived, the $\delta^{18}O_{sw}$ can then provide information about the global ice volume and the local salinity. Moreover, if a foraminifera test is sufficiently well preserved to estimate $\delta^{18}O_{sw}$, then the foraminifera would also be sufficiently well preserved to estimate temperature if the $\delta^{18}O_{sw}$ term in equation (2) can be determined from an independent source. Problems with disentangling temperature and $\delta^{18}O_{sw}$ are common to all ocean $\delta^{18}O$ archives, including corals [*Watanabe et al.*, 2011], diatoms [*Snelling et al.*, 2014], and molluscs [*Jones and Allmon*, 1995]. For any of these measurements to be utilized, a robust, independent estimate of either $\delta^{18}O_{sw}$ or temperature is required [*Williams et al.*, 2009].

Although less numerous than ocean-based measurements, land-based measurements of Pliocene age $\delta^{18}O$ are also available and include pedogenic carbonates [*Winnick et al.*, 2013], tree rings [*Hill et al.*, 2011; *Csank et al.*, 2013; *Ballantyne et al.*, 2010], and speleothems [*Vaks et al.*, 2013]. Like the ocean-based measurements, $\delta^{18}O_c$ in speleothems incorporate a signal from both temperature and the $\delta^{18}O$ of the source water, meaning that either temperature or the $\delta^{18}O$ of the source water must be estimated by an alternative method to utilize this data. Interpreting the oxygen isotope ratio of tree ring cellulose is subject to a different problem. This is predominantly controlled by the oxygen isotope ratio of the source water to the tree, although it is also affected by evaporative enrichment in the leaves and fractionations during cellulose synthesis [e.g., *Roden et al.*, 2000]. Providing that the $\delta^{18}O$ of the source waters can be determined from tree rings, they can then be related to climate parameters (such as temperature and precipitation) using modern relationships, by assuming that these modern relationships are representative of paleoclimates.

In order to relate Pliocene-aged $\delta^{18}O$ measurements to climate, an answer to one of two important questions is required. If $\delta^{18}O_p$ or $\delta^{18}O_{sw}$ can be obtained, the question is "How were water isotopes in precipitation or seawater related to standard climate variables (temperature, precipitation, and salinity) in the Pliocene?" Alternatively, if it is necessary to disentangle a temperature signal from $\delta^{18}O_p$ or $\delta^{18}O_{sw}$ within an observation, it is necessary to know "What were $\delta^{18}O_p$ and $\delta^{18}O_{sw}$ during the Pliocene?" Both of these questions can be addressed in this paper because the processes governing $\delta^{18}O$ throughout the hydrological cycle are well understood and have been incorporated into climate models [*Joussaume et al.*, 1984; *Jouzel et al.*, 2000; *Mathieu et al.*, 2002; *Noone and Simmonds*, 2002; *Lee et al.*, 2007; *Risi et al.*, 2010; *Werner et al.*, 2011] including complex atmosphere-ocean general circulation models (GCMs) [*Schmidt et al.*, 2007; *Zhou et al.*, 2008; *Tindall et al.*, 2009]. These models have been used to investigate climates including the mid-Holocene [e.g., *Hoffmann et al.*, 2000], the Last Glacial Maximum [e.g., *Hoffmann et al.*, 2000], the Last Interglacial [*Sime et al.*, 2013], and the Paleogene [*Zhou et al.*, 2008; *Tindall et al.*, 2010; *Roberts et al.*, 2011].

Here the first simulations of the Pliocene climate using a model equipped with $\delta^{18}O$ tracers will be presented. The results from these simulations can be used to address Pliocene-aged $\delta^{18}O$ measurements. The purpose of this paper is to provide a reference for future studies that measure oxygen isotopes in Pliocene-aged climate archives. It will provide modeled estimates of $\delta^{18}O$ in seawater that can be used to either (a) aid in the interpretation of ocean-based temperature proxies or (b) be compared with $\delta^{18}O_{sw}$ obtained from paired measurements of Mg/Ca and $\delta^{18}O_c$. To this end, we will also discuss the relationship between $\delta^{18}O_{sw}$ and

salinity for the Pliocene climate. To facilitate the interpretation of land-based measurements, modeled estimates of $\delta^{18}O_p$ are included. It will be shown how these relate to more widely used climate parameters, such as Pliocene temperature and precipitation, in order to provide a physically based framework for interpreting land-based measurements.

The layout of this paper is as follows: section 2 will describe the model and simulations used, and section 3 will present modeled values of $\delta^{18}O$ in seawater and $\delta^{18}O$ in precipitation for the Pliocene. A quantitative discussion of the relationships between $\delta^{18}O$ and climate will be addressed in sections 4 (for $\delta^{18}O_p$) and 5 (for $\delta^{18}O_{sw}$). The paper is summarized in section 6.

2. Methods

2.1. Model Description

The model used in this study is the Hadley Centre General Circulation Model (HadCM3) [*Gordon et al.*, 2000; *Pope et al.*, 2000] with water isotope tracers included throughout the hydrological cycle [*Tindall et al.*, 2009]. HadCM3 is a general circulation model (GCM) that has been used in many scientific studies including the IPCC 4th assessment report [*Solomon et al.*, 2007]. Although it is no longer state-of-the-art, having been superseded by the HadGEM family of earth system models [*Collins et al.*, 2011; *Hewitt et al.*, 2011], HadCM3 is the optimal tool for this study. The complexity of the HadGEM models means that it is not feasible to use them in a study, such as this, which requires a millennial scale model simulation.

HadCM3 has a resolution of 3.75° × 2.5° with 19 vertical levels in the atmosphere and 1.25° × 1.25° with 20 vertical levels in the ocean. It uses the *Gregory and Rowntree* [1990] convection scheme, a large-scale cloud scheme based on *Smith* [1990] with modifications described by *Gregory and Morris* [1996] and the *Edwards and Slingo* [1996] radiation scheme. In the ocean HadCM3 comprises a simple sea ice model, which is based on the zero-layer model of *Semtner* [1976] (and includes ice drifts, leads, and snow cover). The version of HadCM3 used here comprises the MOSES2 land surface exchange scheme which includes the TRIFFID dynamic vegetation model [*Cox et al.*, 1999], such that the vegetation will fully interact with the climate.

HadCM3 has been used in a number of studies of the mPWP and in particular has been run as part of PlioMIP [*Bragg et al.*, 2012; *Haywood et al.*, 2013a]. It is generally in good agreement with reconstructions, although it does underpredict the Pliocene sea surface temperature (SST) warming over the North Atlantic region [*Prescott et al.*, 2014] and the Northern Hemisphere high-latitude terrestrial warming [*Salzmann et al.*, 2013].

The oxygen isotope component of HadCM3 has been shown to provide a good representation of $\delta^{18}O_{sw}$ and $\delta^{18}O_p$ for the preindustrial climate [*Tindall et al.*, 2009], and it has been used to investigate a number of paleoclimates such as the 8.2ka event [*Tindall and Valdes*, 2011], the Last Interglacial [*Sime et al.*, 2013], and the Eocene [*Tindall et al.*, 2010]. The oxygen isotope component of HadCM3 has also been used to interpret coral records for the preindustrial period [*Russon et al.*, 2013].

2.2. Experimental Design

The mPWP simulation with $\delta^{18}O$ tracers was initialized from a standard preindustrial $\delta^{18}O$ simulation which had been run for several millennia. The preindustrial experiment was then reconfigured into a PlioMIP experiment [*Bragg et al.*, 2012] by changing the ice sheets, the orography, and vegetation parameters according to PRISM3D [*Dowsett et al.*, 2010]; river outflow points and continental configuration were kept as preindustrial. Although using a preindustrial continental configuration instead of a Pliocene configuration could have a small impact on ocean circulation and therefore the spatial distribution of $\delta^{18}O_{sw}$, the impact should be relatively minor since the continental configuration of the mPWP is reasonably close to modern. Following the PlioMIP protocol, CO_2 levels were set to 405ppmv and orbital parameters were set to 3.205Ma. For model-data comparison 3.205Ma was chosen as a Pliocene time slice, because the orbital parameters are close to modern and climate is relatively stable for the precession cycle centered on this time [*Haywood et al.*, 2013b]. Initial vegetation patterns for the Pliocene were prescribed from PRISM3; however, HadCM3 used dynamic vegetation such that the relative proportions of different vegetation types at the end of a long simulation are unrelated to the initial vegetation patterns used. Although output from the TRIFFID model cannot be directly compared with Pliocene vegetation reconstructions [*Salzmann et al.*, 2013] which are presented as biomes, the results from this simulation have been converted to biomes using BIOME4 [*Kaplan*, 2001] and are presented in *Pound et al.* [2014].

Both the $\delta^{18}O_{sw}$ and salinity values of the ocean were initialized from the preindustrial simulation, because this represented a previously spun-up system. In reality, the Pliocene ice sheets reduction of ≈ 1/3 relates to a sea level rise of 28m, a reduction of mean ocean salinity of 0.25psu, and a reduction of mean ocean $\delta^{18}O_{sw}$ of 0.3‰. Therefore, mPWP values of salinity and $\delta^{18}O_{sw}$ are obtained by subtracting 0.25psu and 0.3‰ from all values at a postprocessing stage. Although there is some uncertainty over the true value of Pliocene sea level, the value of 28m used here is slightly higher than suggested by *Miller et al.* [2012] and *Stocker et al.* [2013]; therefore, the values of 0.25psu and 0.3‰ could be reduced, if required, to provide information about alternate scenarios with different ice sheet configurations.

The mPWP HadCM3 simulation and a parallel preindustrial simulation were run for 2500years, and results are presented from the final 30years.

3. Mean $\delta^{18}O$ Values for the mPWP

3.1. Seawater $\delta^{18}O$

Figure 1 shows the Pliocene ocean surface mean $\delta^{18}O_{sw}$ averaged over the last 30years of the experiment both in absolute terms (Figure 1a) and as an anomaly from the preindustrial simulation (Figure 1b). (Preindustrial $\delta^{18}O_{sw}$ predicted by the model is compared to observations in *Tindall et al.* [2009]). Model predictions suggest that for most of the globe the spatial patterns of $\delta^{18}O_{sw}$ were very similar between the Pliocene and the preindustrial period, and therefore, $\delta^{18}O_{sw}$ could be estimated based on the global ice volume. However, there are regional differences, and paleodata from these regions should be interpreted by including uncertainties in $\delta^{18}O_{sw}$. The most notable difference is over the Arctic Ocean where the model suggests that Pliocene $\delta^{18}O_{sw}$ was up to 1‰ lower than would be estimated by correcting the preindustrial with Pliocene ice volume. Over a region of the South Atlantic $\delta^{18}O_{sw}$ is up to 0.3‰ higher than would be obtained from correcting with ice volume, and in several coastally trapped regions (namely, the eastern coasts of Asia and India and the region around Antarctica), the model suggests that $\delta^{18}O_{sw}$ was 0.1‰ to 1‰ lower.

Over the Mediterranean the model suggests that $\delta^{18}O_{sw}$ is 0.3‰ higher than the ice volume would suggest. (Since the ice volume correction used is −0.3‰, this coincidentally suggests that Mediterranean $\delta^{18}O_{sw}$ at 3.205Ma could have been close to the preindustrial values). The spatial resolution of HadCM3 is too coarse to explicitly include the exchange of water between the Mediterranean and the North Atlantic (the exchange being parametrized through use of a "diffusive pipe"), and so this result must be treated with caution. However, for the modern, both the exchange between the Mediterranean and the Atlantic and the salinity of the inflow and outflow waters are comparable to observations [see *Ivanovic et al.*, 2013], adding confidence to these results. In a warmer world, where the hydrological cycle is more intense, it is likely that both salinity and $\delta^{18}O_{sw}$ gradients between the Mediterranean and the Atlantic will be stronger; hence, the more enriched $\delta^{18}O_{sw}$ in the Mediterranean that we see in this simulation is reasonable.

Since climate proxies may not represent annual mean conditions but instead can represent a particular season, seasonal variability of $\delta^{18}O_{sw}$ is also considered. Figure 2 shows the difference in modeled Pliocene $\delta^{18}O_{sw}$ from the annual mean value for each season, December-January-February (DJF), March-April-May (MAM), June-July-August (JJA), and September-October-November (SON). It is seen that over most of the ocean, $\delta^{18}O_{sw}$ does not vary throughout the year; however, in most coastal regions it is necessary to consider the season that the climate proxy represents. In general, HadCM3 suggests that Northern Hemisphere coastal regions are up to 0.5‰ enriched in $\delta^{18}O_{sw}$ (relative to the annual mean) in DJF and MAM but depleted by up to 0.5‰ (relative to the annual mean) in JJA and SON. In the Southern Hemisphere this pattern is reversed and usually weaker. A very similar seasonal pattern of $\delta^{18}O_{sw}$ appears in the preindustrial HadCM3 simulation (not shown), implying that there are no factors specific to the mPWP climate that are causing this variability. Therefore, to interpret data close to 3.205Ma (which corresponds to the orbital configuration used), it is reasonable to use modern observations of the seasonal distribution of $\delta^{18}O_{sw}$; however, a different orbital configuration could lead to a different pattern of $\delta^{18}O_{sw}$ seasonal distribution in coastal regions. The need to focus on a relatively short time slice for model comparisons and data synthesis was discussed by *Haywood et al.* [2013b] and implies that these results are only directly applicable to the 3.205Ma time slice which was used in this simulation. The patterns shown in Figure 2 are related to the amount of surface and subsurface runoff from the land in various seasons. There is more runoff from the land surface in the summer season, and since runoff originates from meteoric waters it is more depleted in $\delta^{18}O$ than the ocean water. The runoff therefore leads to a small reduction in $\delta^{18}O_{sw}$ close to the coast. This reduction will be amplified in those

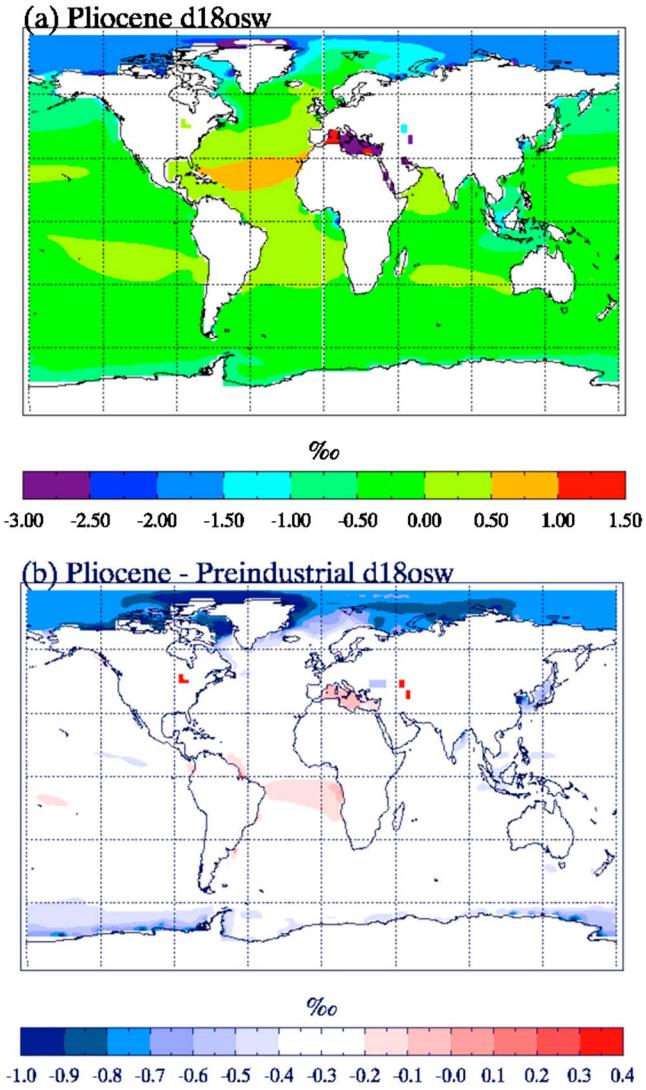

Figure 1. Pliocene $\delta^{18}O_{sw}$ as predicted by HadCM3 (a) absolute values and (b) difference from preindustrial values.

seasons where there is more precipitation and hence more runoff; however, it is noted that the model resolution (3.75° × 2.5°) is not high enough to simulate the full amplitude of the seasonal cycle close to the coast. It is also noted that the river outflow points in the Pliocene simulation are the same as in the preindustrial simulation and that large changes in river outflow could affect the location of changes in coastal $\delta^{18}O_{sw}$.

3.2. The $\delta^{18}O$ in Precipitation

Figure 3 shows $\delta^{18}O$ in precipitation ($\delta^{18}O_p$) for the Pliocene and the $\delta^{18}O_p$ anomaly between the Pliocene and the preindustrial values. In general, Pliocene $\delta^{18}O_p$ was enriched at high latitudes and depleted in the tropics relative to the preindustrial values, leading to a smaller equator to pole $\delta^{18}O_p$ gradient in the Pliocene. This follows the temperature change (Figure 4a) where polar amplification of temperature change means that the modeled equator to pole temperature gradient was reduced in the Pliocene. The standard interpretation of $\delta^{18}O_p$ is that it is directly related to temperature at high latitudes and inversely related to precipitation at low latitudes [*Dansgaard*, 1964], the inverse relationship with precipitation being commonly known as the "amount effect." This standard interpretation appears to apply for the Pliocene-preindustrial $\delta^{18}O_p$ anomaly, to a certain extent. For example, over Antarctica, Greenland, Western Canada, Alaska, and Eastern Russia, the increase in $\delta^{18}O_p$ in the Pliocene simulation can be directly related to the warmer temperatures in these regions. However, over the remainder of northern Eurasia, there is a notable increase in temperature with only a small increase in $\delta^{18}O_p$, showing that the standard linear interpretation is not always valid.

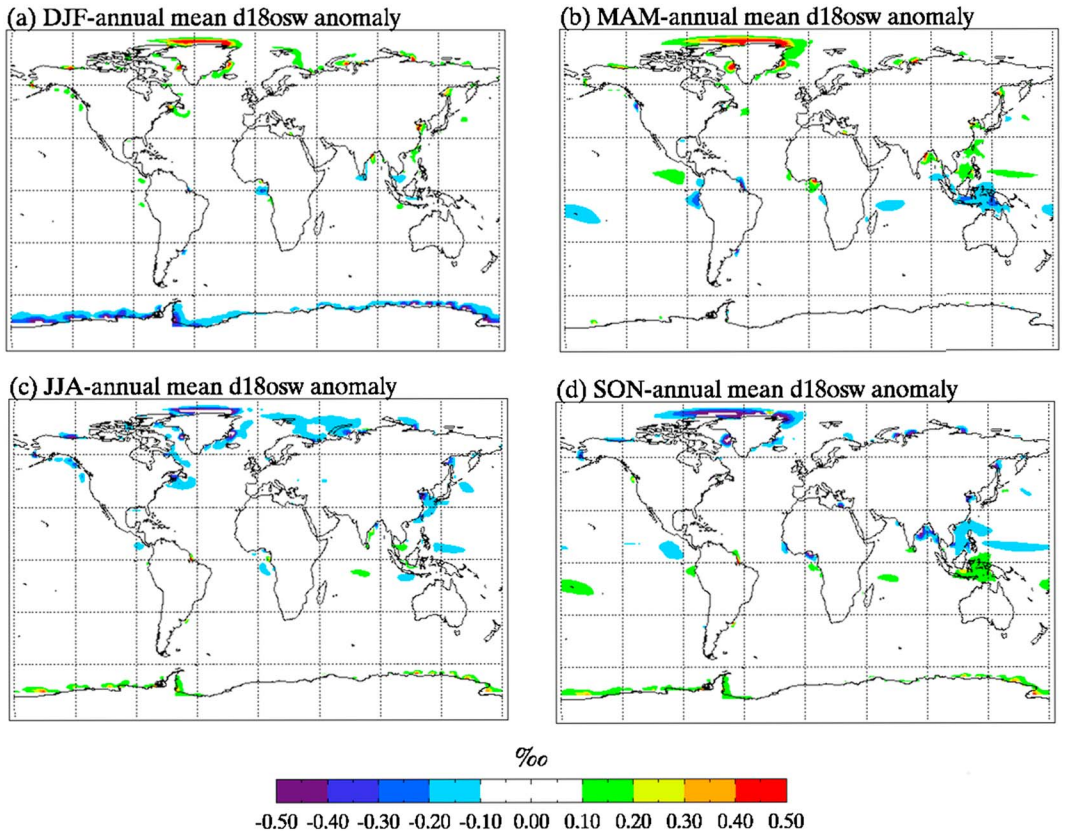

Figure 2. Difference between the seasonal and annual values of the Pliocene-preindustrial $\delta^{18}O_{sw}$ anomalies.

At lower latitudes, the $\delta^{18}O_p$ anomaly (seen in Figure 3b) is inversely related to precipitation amount (Figure 4b) over many regions. In accordance with expected changes in the hydrological cycle in a warmer world [*Broecker and Putnam*, 2013] the Pliocene Intertropical Convergence Zone (ITCZ) is generally stronger, narrower, and shifted northward relative to that in the preindustrial period. These ITCZ changes are usually (but not always) visible in $\delta^{18}O_p$, with reduced $\delta^{18}O_p$ over large parts of the tropical region associated with the stronger ITCZ. Over the South Atlantic, the reduction in precipitation (due to the northward ITCZ shift) is clearly visible in $\delta^{18}O_p$; indeed, this is the only tropical feature in $\delta^{18}O_p$ that has a notable effect on the $\delta^{18}O_{sw}$ (Figure 1b). Comparing Figures 3b and 4b further, we see that there is not a clear one-to-one correspondence between precipitation amount and $\delta^{18}O_p$ over tropical regions. For example, in the Pacific and Indian Oceans, the increase in rainfall is associated with a corresponding decrease in $\delta^{18}O_p$; however, just north of the equatorial Atlantic there is an increase in rainfall that does not affect $\delta^{18}O_p$. In tropical regions $\delta^{18}O_p$ is determined by local conditions and moisture convergence [*Lee et al.*, 2009]; hence, it appears that the increased precipitation falling just north of the Atlantic is not depleted in $\delta^{18}O$ because the decrease in rainfall upstream of this location would increase the $\delta^{18}O$ in vapor reaching this area. Over the tropics, the relationship between the $\delta^{18}O_p$ anomaly and the local precipitation anomaly between the Pliocene and the preindustrial period is statistically significant ($p < 0.0001$); however, the correlation is low, such that local precipitation amount only explains about 20% of the variability in local $\delta^{18}O_p$. The $\delta^{18}O_p$ is more strongly correlated with regional preciptitation, such that 48% of the variability in local tropical $\delta^{18}O_p$ is explained by the average precipitation over the area within 25° of the gridbox. A more quantitative discussion of the relationship between $\delta^{18}O_p$ and precipitation amount is included in section 4.

Over land there are notable reductions in $\delta^{18}O_p$ over a large region north of the Indian ocean which covers much of southern Asia. However, while the $\delta^{18}O_p$ reduction over China can be related to the direct effect of the East Asian monsoon being stronger in the Pliocene than in the preindustrial period [*Zhang et al.*, 2013] and changes near the equator can be attributed to the changes in the ITCZ, in many regions of South Asia a reduction in $\delta^{18}O_p$ is seen that is not related to local changes in temperature or precipitation. Figure 4b shows no visible differences in precipitation patterns over the Arabian Peninsula due to this region being very dry

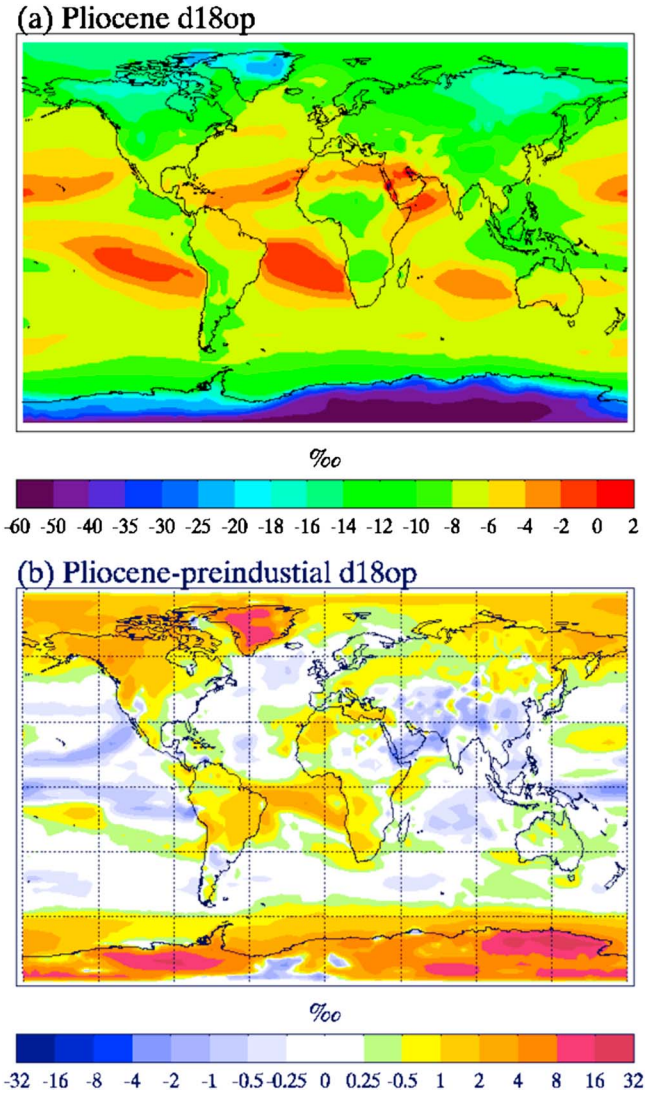

Figure 3. (a) Modeled Pliocene $\delta^{18}O_p$ and (b) modeled Pliocene-preindustrial $\delta^{18}O_p$ anomaly.

and a change in precipitation of less than 2mm/month being too small for the plotting scale. Further analysis shows that HadCM3 simulates a reduction of rainfall of 20–40% in the Pliocene which extends in a band over the north of Africa, Arabia, and southwest Asia. If the local amount effect were dominant in determining $\delta^{18}O_p$ in these regions then an increase in $\delta^{18}O_p$ would result, which is in contrast to what the model shows. It is therefore suggested that the reduced $\delta^{18}O_p$ over Arabia and southwest Asia that occurs without a corresponding local precipitation increase is related to the increase in precipitation upstream of this region, which leaves the water vapor reaching this region depleted in $\delta^{18}O$ relative to today. A GCM that was equipped with water-tagging tracers to analyze the source regions of meteoric waters (as was done by *Vuille et al.*, 2003 [2003]) would be able to investigate this hypothesis more fully.

4. Quantitative Relationship Between $\delta^{18}O_p$ and Climate

One of the aims of this paper is to understand the relationship between $\delta^{18}O_p$ and climate for the Pliocene; hence, this will now be considered quantitatively. The $\delta^{18}O_p$-precipitation amount relationship (the amount effect) is known to hold spatially [*Dansgaard*, 1964], although it does not apply everywhere. For example, over China the determining controls of $\delta^{18}O_p$ vary regionally and include local and upstream condensation over SE China and evaporative enrichment of falling raindrops over NW China [*Lee et al.*, 2012]. Here it is found that the tropical Pliocene minus preindustrial $\delta^{18}O_p$ anomaly at a gridbox is better correlated with the

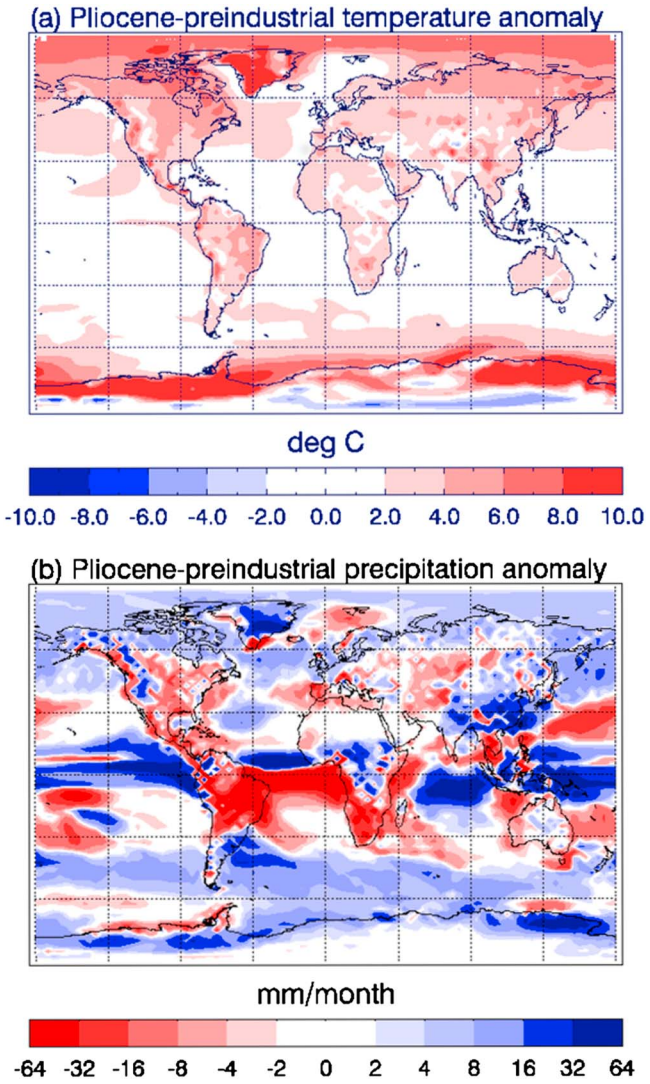

Figure 4. (a) Modeled Pliocene-preindustrial temperature anomaly and (b) modeled Pliocene-preindustrial precipitation anomaly.

regional precipitation anomaly (defined as precipitation occurring within 25° of a site; $R^2 = 0.48$) than the local precipitation anomaly (defined as precipitation occurring in that gridbox; $R^2 = 0.22$). This is because the $\delta^{18}O_p$ anomaly is usually offset from the precipitation anomaly to which it relates. The exact nature of this offset varies by region (Figure 5). Over the Indian and Atlantic Oceans the $\delta^{18}O_p$ anomaly occurs to the south of the precipitation anomaly. Over South America the $\delta^{18}O_p$ anomaly and precipitation anomaly coincide, while in the Pacific Ocean there is a general pattern of reduced $\delta^{18}O_p$ and increased precipitation, which are neither locally related or offset in any direct or obvious way (see Figure 5d). The relationship is such that absence of a $\delta^{18}O_p$ signal does not imply absence of a local climate signal, and data from a number of sites over a region would be needed in order to hypothesize about the regional and local precipitation patterns. Such data may be difficult to obtain for the Pliocene. However, the relationship between $\delta^{18}O_p$ and tropical precipitation is discussed here for completeness and because it may also apply to more recent climates where climate proxy data are more abundant.

Areas of $\delta^{18}O_p$ which are related to tropical precipitation changes are highlighted in Figures 5a–5e by the thick black lines. Boundaries of each area are determined according to where the amplitude of the $\delta^{18}O_p$ signal is less than 0.5‰ or the amplitude of the precipitation signal is less than 15mm/month. To quantify the $\delta^{18}O_p$-precipitation amount relationship, we therefore calculated the maximum and mean $\delta^{18}O_p$ change for each highlighted area; these values are shown in Figure 5f for $\delta^{18}O_p$ (red) and precipitation amount

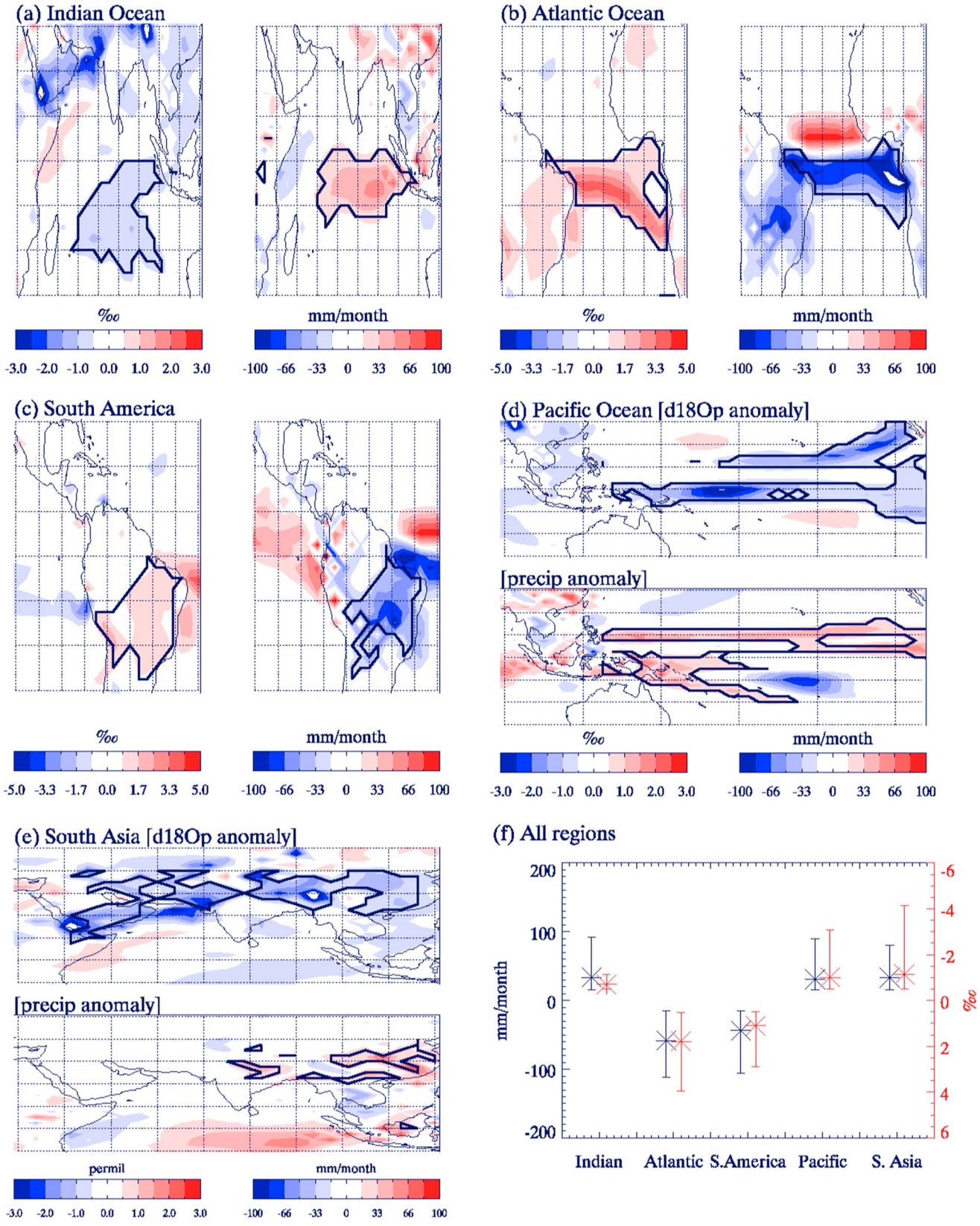

Figure 5. (a–e) Relationship between $\delta^{18}O_p$ anomalies and precipitation anomalies on a regional basis. (f) The range of precipitation and $\delta^{18}O_p$ anomalies that are enclosed by the thick black lines for each region.

Table 1. Spatial Linear Relationships Between $\delta^{18}O_p$ and Temperature for the Pliocene and Preindustrial According to the Equation $T = (\text{slope} \times \delta^{18}O_p) + \text{Intersect}$[a]

	Intersect	Slope	r^2	Modern Explvar
		Preindustrial		
Asia	16	3.1	0.83	
Antarctica	7	0.6	0.87	
North America	20	2.8	0.69	
Europe	28	4.2	0.81	
Greenland	−18.0	0.76	0.26	
		Pliocene		
Asia	19	3.3	0.78	0.76
Antarctica	24	0.95	0.86	0.66
North America	27	3.3	0.80	0.77
Europe	32	4.4	0.86	0.80
Greenland	−8.0	1.2	0.44	0.21

[a]For the Pliocene "modern explvar" shows the proportion of temperature variability explained when using the modern relationship instead of the regression calculated from the Pliocene. The relationships have been derived separately for each continent, and only sites poleward of 30° have been used to calculate the regressions.

(black). Crosses denote the mean values, while the error bars denote the range of values (minimum values being defined by the boundaries). This analysis gives a very strong relationship between $\delta^{18}O_p$ and precipitation amount ($R^2 = 0.9$; when mean and maximum values are included). The relationships are reasonably consistent between different regions. Mean relationships are calculated as follows: Pacific = −31 mm month^{-1}‰$^{-1}$, Atlantic = −33 mm month^{-1}‰$^{-1}$, South America = −40 mm month^{-1}‰$^{-1}$, Indian = −48 mm month^{-1}‰$^{-1}$, and South Asia = −29 mm month^{-1}‰$^{-1}$. Relationships between the maximum signals are calculated as follows: Pacific = −29 mm month^{-1}‰$^{-1}$, Atlantic = −28 mm month^{-1}‰$^{-1}$, South America = −30 mm month^{-1}‰$^{-1}$, Indian = −80 mm month^{-1}‰$^{-1}$, and South Asia = −20 mm month^{-1}‰$^{-1}$. These are much larger than the local best fit $\delta^{18}O_p$ anomaly-precipitation amount anomaly relationship (−14 mm month^{-1}‰$^{-1}$). The strong and relatively consistent relationships between $\delta^{18}O_p$ and tropical precipitation amount suggests that if enough $\delta^{18}O_p$ samples could be obtained, past precipitation amount could be quantitatively obtained from $\delta^{18}O_p$ with a reasonable level of accuracy. However, local precipitation at a single site could not be reasonably determined from local $\delta^{18}O_p$.

At high latitudes, $\delta^{18}O_p$ is predominantly determined by temperature, and hence, the high-latitude temperature-$\delta^{18}O_p$ relationship will be analyzed in two ways. First, we will consider the spatial gradients between $\delta^{18}O_p$ and temperature for the Pliocene and the extent to which these differ from the modern. This analysis is useful for studies which have $\delta^{18}O_p$ observations across a region [e.g., *Winnick et al.*, 2013]. Second, we will consider quantitatively the relationship between the temperature anomaly and the $\delta^{18}O_p$ anomaly for the Pliocene (see Figures 3b and 4a), as this would be more useful for interpreting data at a single site.

The spatial relationship using a least squares regression between temperature and $\delta^{18}O_p$ is shown in Table 1 for the preindustrial and the Pliocene simulations for different regions. This shows the slope and the intersect of the linear $\delta^{18}O_p$-T relationship ($T = a + (b \times \delta^{18}O_p)$) and the coefficient of determinant (r^2). Since the relationships are similar for the Pliocene and for the preindustrial period, Table 1 also shows the amount of Pliocene temperature variance that could be explained by using the modern $\delta^{18}O_p$-T relationship. Over most continents the spatial regression is similar for the Pliocene and the preindustrial period, and using the slope derived from the preindustrial values instead of that derived from the Pliocene is not a major detriment. However, over Greenland and Antarctica it appears detrimental to use the modern relationships to estimate Pliocene temperatures from $\delta^{18}O_p$. Over Antarctica using the modern relationships will reduce the amount of temperature variance that can be explained by $\delta^{18}O_p$ from 86% to 66%, while over Greenland it is reduced from 44% to 21%. Figure 6 shows the relationship between $\delta^{18}O_p$ and temperature from Greenland and Antarctica where red crosses are taken from the Pliocene simulation and black crosses are taken from the

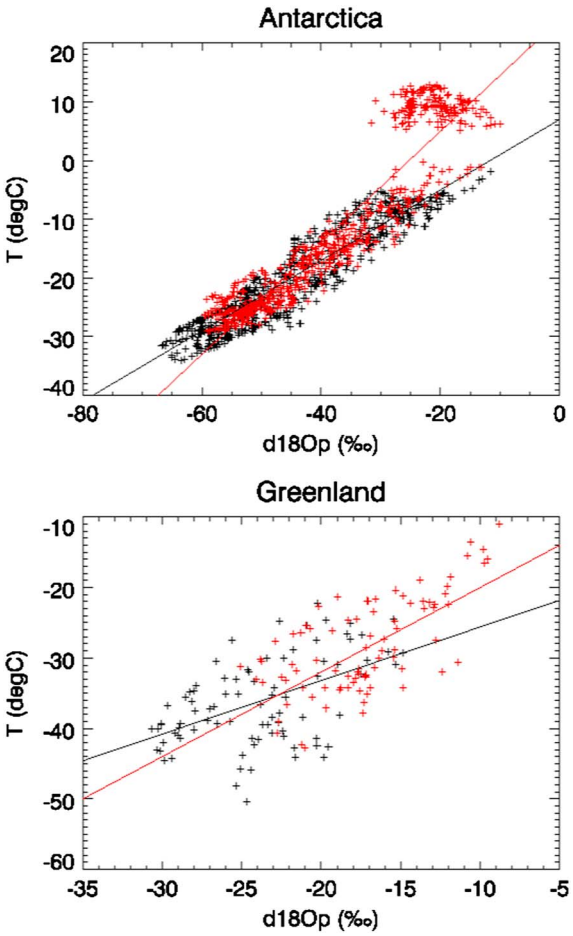

Figure 6. Relationship between $\delta^{18}O_p$ and temperature for Antarctica and Greenland. Red crosses and lines show data and least squares regression equation for the Pliocene. Black crosses and lines show data and least squares regression equation for the preindustrial period.

preindustrial simulation. Over Antarctica the linear relationship between $\delta^{18}O_p$ and temperature is similar for the two climates. The best fit linear relationships for the preindustrial period and the Pliocene are shown by the black and red lines, respectively. However, the relationship becomes problematic for those points in the Pliocene simulation where the temperature is warmer than 5°C. The $\delta^{18}O_p$ for these sites is much lower than would be expected from the linear relationship, and using the preindustrial linear regression for these sites would underpredict the temperature by up to 25°C. On closer inspection these sites represent those Antarctic regions which the PRISM3 data set suggest were ice free in the Pliocene, and the model suggests that these sites were warmer during the summer than the ice-covered part of Antarctica or the Southern Ocean. In contrast, $\delta^{18}O_p$ over these regions is the same as the $\delta^{18}O_p$ over the Ocean near Antarctica, presumably because the vapor reaching Antarctica must have arrived via the Southern Ocean where its isotope composition was modified according to local conditions. The $\delta^{18}O$ in moisture reaching this region is therefore more representative of the coldest conditions the vapor experienced on its trajectory than of local conditions at the site, which are warmer. Points which have changed from being ice covered in the preindustrial period to ice free in the Pliocene do not have $\delta^{18}O_p$ and temperature related in the same way as points which have remained ice covered throughout, as removing ice from a gridbox has a much stronger effect on local temperature than on $\delta^{18}O_p$.

It is perhaps unsurprising that the $\delta^{18}O_p$-temperature relationship changes more between the Pliocene and the preindustrial period over Greenland than it does over any other region. The extent of the Greenland ice sheet in the Pliocene simulation was only about 40% of that in the preindustrial period, and this causes the $\delta^{18}O_p$-temperature relationship to be much stronger in the Pliocene. However, the preindustrial $\delta^{18}O_p$-temperature relationship for ice-free points ($T = -2.3 + (1.6 \times \delta^{18}O_p)$) is closer to the Pliocene relationship and better able to predict Pliocene temperatures throughout Greenland. These simulations suggest that the modern spatial relationships between $\delta^{18}O_p$ and temperature could be used for the Pliocene in those regions where there are no major changes to the boundary conditions (e.g., ice extent) which would affect local $\delta^{18}O_p$ and local temperature in a different way.

Although spatial gradients between $\delta^{18}O_p$ and temperature are similar for the Pliocene and the preindustrial period, this is partly due to the fact that both temperature and $\delta^{18}O_p$ generally decrease with increasing latitude, and the continentality effect on $\delta^{18}O_p$ will be similar for both climates. A more rigorous test on the temperature and $\delta^{18}O_p$ relationship for the Pliocene climate will now be undertaken by comparing the Pliocene-preindustrial anomaly of $\delta^{18}O_p$ with that of temperature over different regions of the globe.

The relationship between the local $\delta^{18}O_p$ anomaly and the local temperature anomaly is relatively weak, even over regions where the spatial relationship is strong. For example, the model suggests $R^2 = 0.29$ over Europe, $R^2 = 0.04$ over North America, and $R^2 = 0.37$ over Antarctica. Figure 7 shows the $\delta^{18}O_p$ anomaly and the

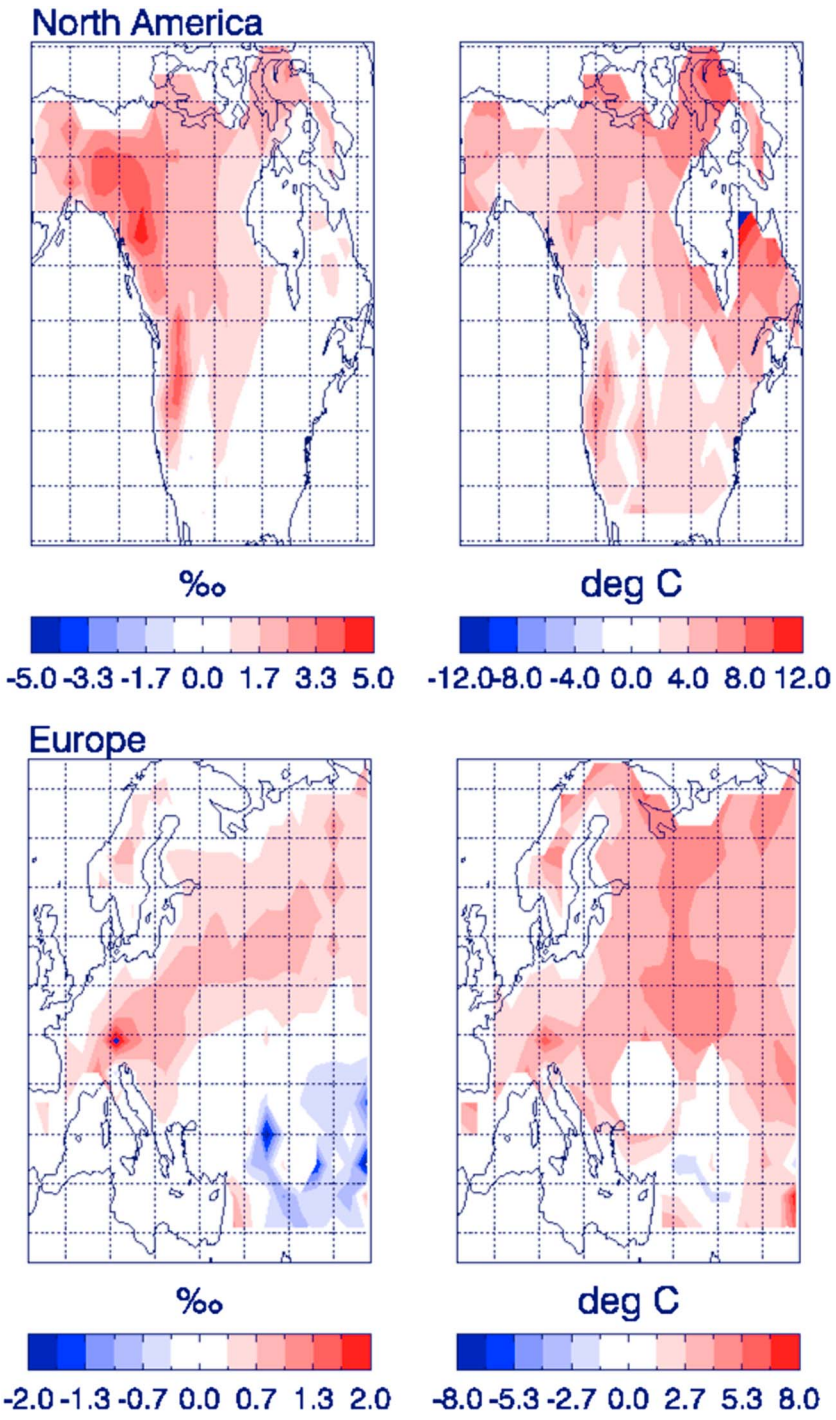

Figure 7. Modeled $\delta^{18}O_p$ anomalies and temperature anomalies over North America and Europe.

temperature anomaly over North America and Europe. It is seen that both continents show a general increase of both $\delta^{18}O_p$ and temperature; however, for neither region does the maximum $\delta^{18}O_p$ signal correspond to the maximum temperature signal and hence the relatively poor local relationship between the two anomalies.

Over North America the maximum $\delta^{18}O_p$ signal occurs to the northwest of the continent, while the south and east of the continent have $\delta^{18}O_p$ relatively unchanged; the maximum temperature anomaly occurs to the northeast. This difference is likely because the precipitation over the northwest originates in the Northern Pacific, which is warmer in the Pliocene simulation (Figure 4a), while the precipitation over the southeast

originates in the equatorial Atlantic, which is relatively unchanged between the simulations, indicating the importance of understanding changes in source water. Changes in temperature, however, are more strongly determined by local factors including changes in snow cover and do not react to the Pliocene boundary conditions in exactly the same way as $\delta^{18}O_p$.

The relationship between $\delta^{18}O_p$ and temperature anomalies for the Pliocene is more complex than any local regression, and there is no obvious formula to relate the two for past climates (despite spatial patterns being strongly correlated). Isotope-enabled simulations such as this can therefore be used to interpret past proxy data and relate the data to climate. If the model $\delta^{18}O_p$ change is consistent with the $\delta^{18}O_p$ change from the data, then the model can be used to analyze possible climate patterns at that time, not just local to the site but over a much larger region.

The isotope-enabled Pliocene simulation can be used as an independent way of relating $\delta^{18}O_p$ to temperature at high latitudes. For example, tree ring data over Bylot Island, Canada [*Csank et al.*, 2013] (73°N 78°W), which likely represents a snapshot of an interglacial period within the Plio-Pliestocene, showed $\delta^{18}O_p$ enriched by 2–6‰ relative to preindustrial values, which was attributed to a mean annual temperature increase of 11.4°C. Model results at this location for the Pliocene interglacial at 3.205Ma show $\delta^{18}O_p$ enriched by 2.2‰, corresponding to temperatures 9.5° warmer than preindustrial values. The relationship between $\delta^{18}O_p$ and temperature inferred from the data for an interglacial Plio-Pliestocene climate is therefore in agreement with that in the model.

However, caution must be taken with applying these $\delta^{18}O_p$ results to all Pliocene-aged climate proxies. For example, Pliocene-aged speleothems from the Negev Desert, Israel [*Vaks et al.*, 2013], showed $\delta^{18}O$ of approximately −9.7 to −11.2‰ and reduced relative to the Pleistocene. HadCM3 does not agree with these data, as HadCM3 simulates $\delta^{18}O_p$ as being 1‰ enriched in this location relative to the preindustrial values. Further analysis reveals that at this location, Pliocene precipitation simulated by HadCM3 was extremely low such that under this precipitation scenario speleothems would not be able to grow at all. Hence, there is a clear mismatch between the model and data in this region, part of which may be due to trying to relate the model simulation which was intended to represent 3.205Ma to wider Pliocene interglacial conditions (see *Prescott et al.* [2014] for a discussion about orbital variability in the Pliocene).

5. The $\delta^{18}O_{sw}$ and Paleosalinity

Figure 8 shows the difference between mPWP sea surface salinity and preindustrial sea surface salinity from HadCM3. The salinity correction due to the global ice volume is −0.25psu; this is close to that estimated by the model over most of the ocean. However, there are also regional hydrological changes, where a global ice volume correction alone is not sufficient to accurately determine the mPWP-preindustrial salinity anomaly. By comparing the mPWP-preindustrial salinity anomaly (Figure 8) with the corresponding $\delta^{18}O_{sw}$ anomaly (Figure 1b), we see that the model suggests a clear relationship between the local salinity anomaly and the $\delta^{18}O_{sw}$ anomaly ($R^2 = 0.64$). This contrasts with $\delta^{18}O_p$ anomalies which were not related to local climate and suggests that $\delta^{18}O_{sw}$ could potentially be used to quantitatively determine local salinity changes.

The existence of a relationship between $\delta^{18}O_{sw}$ and salinity is well known [*Fairbanks et al.*, 1997] and is reasonable since both salinity and $\delta^{18}O_{sw}$ are governed by the hydrological cycle. The $\delta^{18}O_{sw}$ has therefore been used to determine the salinity of the ocean for past climates such as the Pliocene [e.g., *Karas et al.*, 2011; *Beltran et al.*, 2007]. However, the relationship in HadCM3 between salinity and $\delta^{18}O_{sw}$ is not exact, nor is it perfectly linear, even for the relatively small change in climate between the mPWP and the preindustrial period. Some features, such as the low values off the east coast of Asia, are stronger in salinity than in $\delta^{18}O_{sw}$, while high-latitude features appear stronger in $\delta^{18}O_{sw}$. Here we will investigate the extent to which $\delta^{18}O_{sw}$ can be used to derive Pliocene salinity (provided the $\delta^{18}O_{sw}$ signal can be disentangled from the temperature signal in $\delta^{18}O$ archives).

The relationship between $\delta^{18}O_{sw}$ and salinity for the modern period is regionally determined [e.g., *LeGrande and Schmidt*, 2006], and the regional relationship has been applied to past climates such as the Pliocene. However, *De Schepper et al.* [2009] noted that the exact salinity $\delta^{18}O_{sw}$ relationship for the Pliocene is unknown; hence, Pliocene salinity can only be interpreted from $\delta^{18}O_{sw}$ records in terms of relative salinity (i.e., whether salinity was increasing or decreasing through time). While relative salinity changes are useful, it would also be beneficial to have an indication of the possible amplitude of salinity changes for past climates; therefore,

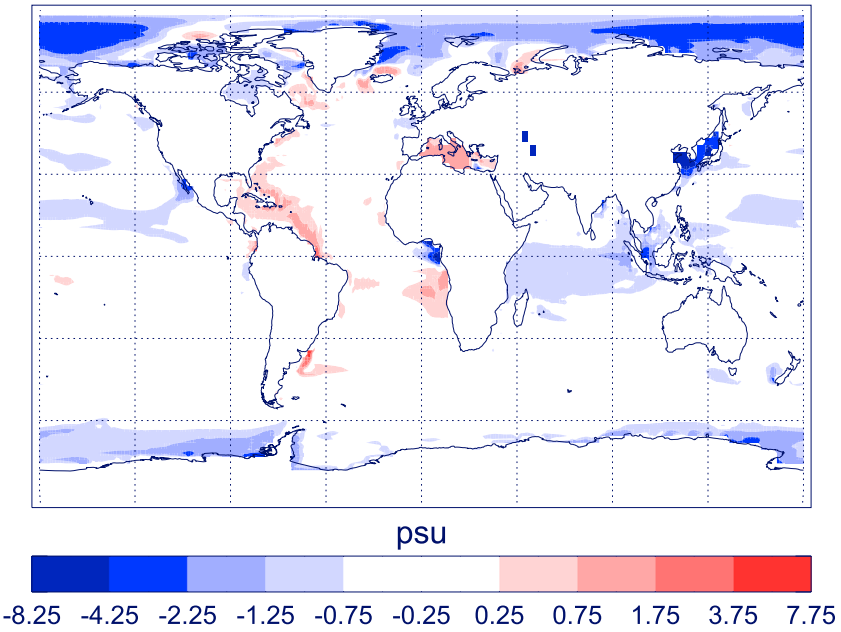

Figure 8. Modeled Pliocene-preindustrial salinity anomaly.

we will use the results herein to investigate the possible quantitative relationship between the two fields and whether this is different from today's.

LeGrande and Schmidt [2006] found the modern relationship between $\delta^{18}O_{sw}$ and salinity over the major ocean basins to have a slope of between 0.15 and 0.55 and an intersect of between −4.6‰ and −19.0‰. This compares well with our model results which were calculated spatially over the globe as

$$\delta^{18}O_{sw} = 0.20 \times \text{salinity} - 6.82: \; r = 0.80. \tag{3}$$

For the Pliocene simulation the relationship is similar but slightly stronger and is

$$\delta^{18}O_{sw} = 0.22 \times \text{salinity} - 7.84: \; r = 0.84. \tag{4}$$

The very strong correlation between $\delta^{18}O_{sw}$ and salinity is due to the fact that both fields are larger at the equator than at the poles.

To assess whether spatial gradients of Pliocene $\delta^{18}O_{sw}$ can be used to estimate spatial patterns of Pliocene salinity, we first compare Pliocene salinity obtained directly from the model (Figure 9a) with Pliocene salinity estimated from modeled $\delta^{18}O_{sw}$ and equation (4) (Figure 9c; the difference between the two is shown in Figure 9b). It can be seen that over most of the globe the salinity is well predicted from $\delta^{18}O_{sw}$, but there are notable errors. The errors in estimating Pliocene salinity in this way are similar to, but slightly larger than, using this method for the preindustrial period (shown in Figure 9d). Hence, to a first approximation, if modern $\delta^{18}O_{sw}$ can correctly predict modern salinity at a location, then it is reasonable to use Pliocene $\delta^{18}O_{sw}$ to estimate Pliocene salinity; however, errors may be larger in the Pliocene.

The mean absolute error (MAE) in salinity estimated using the different methods are now compared. When salinity is estimated according to spatial gradients (Figures 9b and 9c), the MAE = 0.7 psu; however, when salinity is estimated by correcting the modern using a global ice volume correction, the MAE is smaller (0.6psu). Hence, for a climate with a familiar continental configuration, correcting using the global ice volume is a better way of estimating past salinity than using spatial gradients of $\delta^{18}O_{sw}$. However, the spatial gradients could be used as an independent test of salinity estimates.

Since the anomaly patterns of $\delta^{18}O_{sw}$ (Figure 1b) and salinity (Figure 8) are similar, we now consider whether we can use these anomalies to improve on the salinity estimated using the global ice volume correction. The linear relationship between the Pliocene-preindustrial $\delta^{18}O_{sw}$ anomaly ($\delta^{18}O_{sw}$(anom)) and the

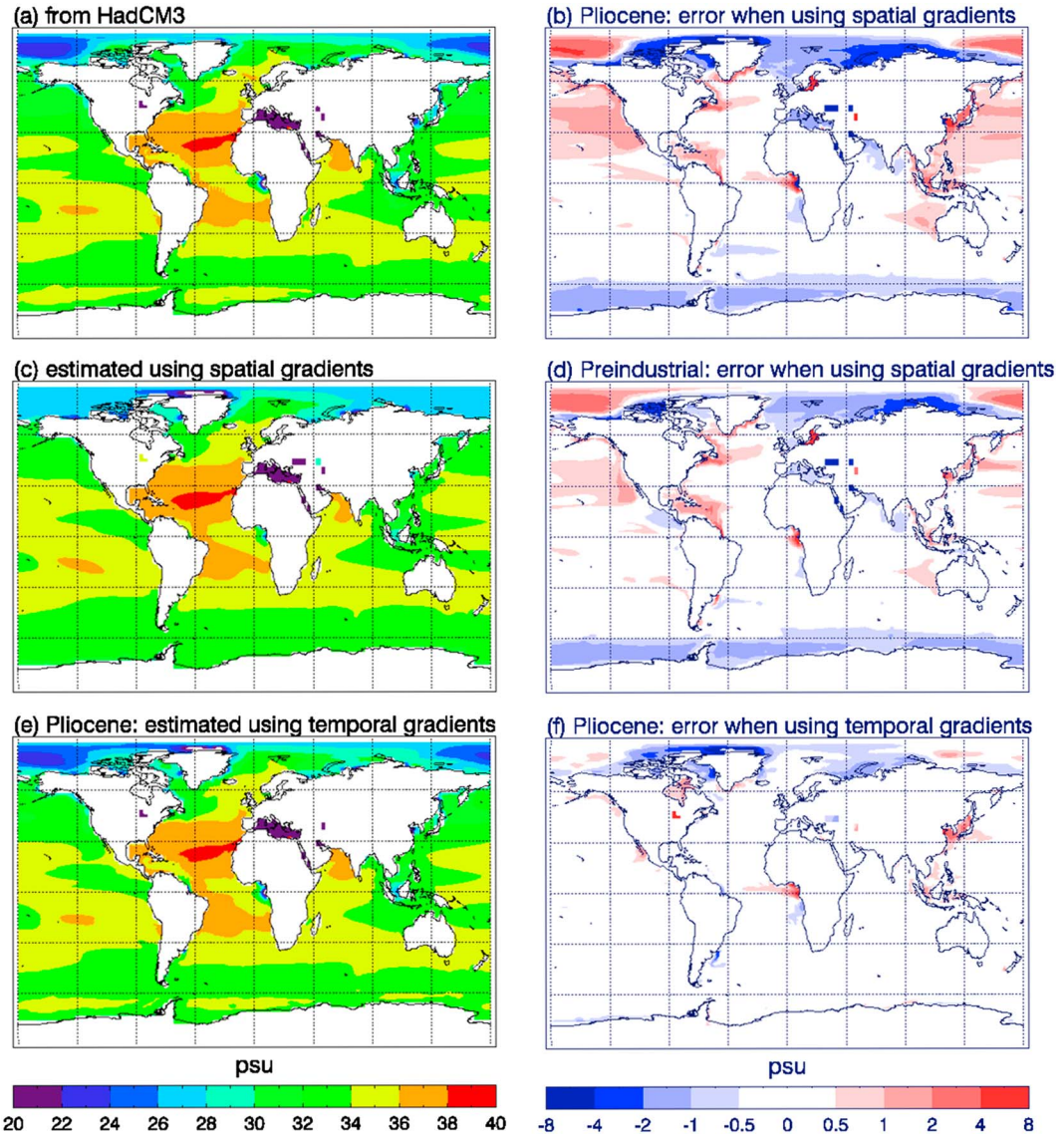

Figure 9. Pliocene salinity (a) from HadCM3, (c) estimated from spatial gradients of $\delta^{18}O_{sw}$, and (e) estimated using the Pliocene-preindustrial $\delta^{18}O_{sw}$ anomalies. Errors in estimated salinity are shown for (b) Pliocene using spatial gradients only, (d) preindustrial period using spatial gradients only, and (f) Pliocene when using the Pliocene-preindustrial $\delta^{18}O_{sw}$ anomaly.

Pliocene-preindustrial salinity anomaly (salinity(anom)) follows the same form as used by *Rostek et al.* [1993] for the Indian Ocean and is calculated globally as

$$\delta^{18}O_{sw}(\text{anom}) = 0.23 \times \text{salinity(anom)} - 0.28\colon\ r = 0.71. \tag{5}$$

The slope of this anomaly relationship (equation (5)) is similar to the slope of the spatial relationships (equations (3) and (4)); hence, HadCM3 suggests that the slope is reasonably robust for these time periods and the anomaly between them. The intersect term in equation (5) is close to what would be estimated from the ice volume correction, which is

$$\frac{\text{intersect}_{\text{expected}} = \delta^{18}O_{\text{swivc}} - \text{sal}_{\text{ivc}}}{\text{slope}}, \tag{6}$$

where sal_{ivc} is the salinity ice volume correction (=−0.25), $\delta^{18}O_{\text{swivc}}$ is the $\delta^{18}O_{sw}$ ice volume correction (=−0.3), and slope is the slope of equation (5) (=0.23). Hence, $\text{intersect}_{\text{expected}}$ is −0.22, which compares

well with the value obtained from the linear regression of −0.28. Using the anomaly relationship to estimate salinity(anom) from $\delta^{18}O_{sw}$(anom) and combining this with modern salinity gives the estimated Pliocene salinity shown in Figure 9e (with the difference from HadCM3 salinity shown in Figure 9f). Using the anomaly method, the MAE = 0.3 and is a substantial improvement over using either the ice volume correction or using spatial gradients. There are some caveats to using the anomaly approach. First, the modern land-sea mask was used in our simulations, and so the true agreement between preindustrial salinity and Pliocene salinity may be less in the real world than it is in the model. Also, these results assume that the relationship between $\delta^{18}O_{sw}$ and salinity is known and is the same as is predicted by the model; if the true relationship between $\delta^{18}O_{sw}$(anom) and salinity(anom) is not known (and instead has to be estimated), this would have a detrimental effect on paleosalinity predictions. However, the consistency of the slope of the $\delta^{18}O_{sw}$-salinity relationship between the Pliocene and the modern period is an encouraging step toward producing more quantitative reconstructions of Pliocene salinity.

6. Summary

In many ways the boundary conditions for modeling the mPWP at 3.205Ma are very similar to those of the preindustrial period, although there are important differences. Carbon dioxide levels have increased substantially, ice sheets are reduced, and there are subtle changes to orography. However, for many PlioMIP experiments (including this one) the land-sea mask is the same as in the preindustrial period (which can lead to similar ocean circulation), and orbital parameters at 3.205Ma are similar (which can lead to similar seasonality). For fields such as $\delta^{18}O_p$ and particularly $\delta^{18}O_{sw}$ the changes in the model's boundary conditions are only sufficient to lead to subtle differences between the preindustrial period and the mPWP. However, this paper has shown that these changes can be important in certain regions and at certain timescales and potential changes must be considered in order to get maximum accuracy from the interpretation of climate proxy data.

This paper has focused on two questions that are needed to help interpret $\delta^{18}O$ data. The first of these is "What values of $\delta^{18}O_{sw}$ and $\delta^{18}O_p$ are expected over the globe for the Pliocene climate?" and is important to disentangle the convoluted signal that is obtained in some $\delta^{18}O$ archives. Model results suggest that Pliocene $\delta^{18}O_{sw}$ was within 0.1‰ of the value expected from a simple ice volume correction over most of the ocean, although there are differences. The most notable of these is the Arctic Ocean, which was subject to increased precipitation in the Pliocene. This precipitation was depleted in $\delta^{18}O_p$ relative to standard ocean water and would reduce the $\delta^{18}O_{sw}$ in that basin. Other regions of difference include the following: enclosed basins (such as the Mediterranean) which are influenced by the more intense hydrological cycle in the Pliocene and as a result are expected to have more enriched $\delta^{18}O_{sw}$ (and increased salinity); the South Atlantic, which is more enriched in $\delta^{18}O_{sw}$ due to the northward shift of the ITCZ; and coastally trapped regions which are affected by the amount of runoff from the land surface. Surface runoff can also lead to seasonal differences in $\delta^{18}O_{sw}$ near the coast and must be taken into account when interpreting seasonal, coastally trapped, $\delta^{18}O$ measurements. HadCM3 suggests that $\delta^{18}O_p$ in ice-free regions was usually within 4‰ of modern values and was enriched relative to today at high latitudes, over parts of South America and Africa, and depleted relative to today over South Asia. However, over the ice sheets the $\delta^{18}O_p$ anomaly was much larger reaching values of up to 25‰.

The second question addressed in this paper was "What is the relationship between $\delta^{18}O$ and climate for the Pliocene?" or more specifically "What information about climate is available after we have disentangled $\delta^{18}O_p$ or $\delta^{18}O_{sw}$ from an archive?" For $\delta^{18}O_p$, the answer to this question varies spatially. Over the tropics we find a clear relationship between $\delta^{18}O_p$ and precipitation, but the precipitation signal is usually offset from the $\delta^{18}O_p$ signal. Because of this, the absence of a $\delta^{18}O_p$ signal does not imply the absence of a local precipitation signal. It is suggested that data from a number of sites is necessary to provide inferences about Pliocene regional or local precipitation. Where evidence of regional $\delta^{18}O_p$ changes can be found, the size of the precipitation change can be approximated. However, a model such as the isotope-enabled version of HadCM3 would be needed to provide information about the locations of the precipitation change.

The spatial relationship between $\delta^{18}O_p$ and high-latitude temperature over continents in the Pliocene is relatively strong and is similar to that in the modern period. Hence, this study implies that the modern spatial $\delta^{18}O_p$-temperature relationship could be used to quantitatively estimate temperature gradients over a region. However, the local relationship between the $\delta^{18}O_p$ anomaly and the temperature anomaly is relatively weak, and model simulations such as those included here could be invaluable for interpreting preindustrial-Pliocene $\delta^{18}O_p$ anomalies at high latitudes.

Since the present-day continental configuration was used in these experiments, there are not large changes in the spatial patterns of $\delta^{18}O_{sw}$ or salinity between the two climates. These simulations suggest that a reasonable estimate of salinity can be obtained using a combination of a global ice volume correction and a salinity anomaly which has been determined from the $\delta^{18}O_{sw}$ anomaly. However, this method of estimating paleosalinity may not hold for climates with very different orbital configurations or paleogeographies, and a more complex method, such as that suggested by *Rohling* [2007] and *LeGrande and Schmidt* [2011], may be needed.

The changes in $\delta^{18}O_p$ and $\delta^{18}O_{sw}$ between the preindustrial period and the Pliocene are not usually large and are not always related to climate in an obvious way. Yet the estimates provided here, and their relationship to climate, will be useful for interpreting the large amount of $\delta^{18}O$ data that has been collected in the past and which continues to be collected. This would include data from tree rings, corals, and foraminifera. The results here can also facilitate a more accurate model/data comparison. For example, it was previously noted that $\delta^{18}O$ measurements are often paired with Mg/Ca measurements from the same foraminifera test in order to estimate temperature (from Mg/Ca) and $\delta^{18}O_{sw}$ (from the foraminifera $\delta^{18}O$). While previously the temperature could be compared with model results in order to assess model-data agreement, the results herein would allow an additional and independent model-data comparison based on $\delta^{18}O_{sw}$. This would lead to an enhanced and more accurate model-data comparison, which could highlight agreement or problems with either the model and the data and help to take forward our understanding of the Pliocene climate.

Acknowledgments
Research leading to these results has received funding from the European Research Council under the European Union's Seventh Framework Programme(FP7/2007-2013)/ERC grant agreement 278636. The authors would like to thank Jung-Eun Lee, Ruza Ivanovic, and an anonymous reviewer for useful comments on an earlier version of this manuscript and Steven Pickering for model support. Data used to produce the results of this paper are attached as supporting information.

References

Ballantyne, A. P., D. R. Greenwood, J. S. S. Damste, A. Z. Csank, J. J. Eberle, and N. Rybczynski (2010), Significantly warmer Arctic surface temperatures during the Pliocene indicated by multiple independent proxies, *Geology*, *38*(7), 603–606, doi:10.1130/G30815.1.

Beltran, C., M. de Rafelis, F. Minoletti, M. Renard, M. A. Sicre, and U. Ezat (2007), Coccolith delta O-18 and alkenone records in middle Pliocene orbitally controlled deposits: High-frequency temperature and salinity variations of sea surface water, *Geochem. Geophys. Geosyst.*, *8*, Q05003, doi:10.1029/2006GC001483.

Bemis, B. E., H. J. Spero, J. Bijma, and D. W. Lea (1998), Reevaluation of the oxygen isotopic composition of planktonic foraminifera: Experimental results and revised paleotemperature equations, *Paleoceanography*, *13*(2), 150–160, doi:10.1029/98PA00070.

Bragg, F. J., D. J. Lunt, and A. M. Haywood (2012), Mid-Pliocene climate modelled using the UK Hadley Centre Model: PlioMIP Experiments 1 and 2, *Geosci. Model Dev.*, *5*(5), 1109–1125, doi:10.5194/gmd-5-1109-2012.

Broecker, W. S., and A. E. Putnam (2013), Hydrologic impacts of past shifts of Earth's thermal equator offer insight into those to be produced by fossil fuel CO_2, *Proc. Natl. Acad. Sci. U.S.A.*, *110*(42), 16,710–16,715.

Collins, W. J., et al. (2011), Development and evaluation of an Earth-System model-HadGEM2, *Geosci. Model Dev.*, *4*(4), 1051–1075, doi:10.5194/gmd-4-1051-2011.

Cox, P., R. A. Betts, C. B. Bunton, R. L. H. Essery, P. R. Rowntree, and J. Smith (1999), The impact of new land surface physics on the GCM simulation of climate and climate sensitivity, *Clim. Dyn.*, *15*(3), 183–203.

Csank, A. Z., D. Fortier, and S. W. Leavitt (2013), Annually resolved temperature reconstructions from a late Pliocene-early Pleistocene polar forest on Bylot Island, Canada, *Palaeogeogr. Palaeoclimatol. Palaeoecol.*, *369*, 313–322.

Dansgaard, W. (1964), Stable isotopes in precipitation, *Tellus*, *16*(4), 436–468.

De Schepper, S., M. J. Head, and J. Groeneveld (2009), North Atlantic Current variability through marine isotope stage M2 (circa 3.3 Ma) during the mid-Pliocene, *Paleoceanography*, *24*, PA4206, doi:10.1029/2008PA001725.

Dolan, A. M., A. M. Haywood, D. J. Hill, H. J. Dowsett, S. J. Hunter, D. J. Lunt, and S. J. Pickering (2011), Sensitivity of Pliocene ice sheets to orbital forcing, *Palaeogeogr. Palaeoclimatol. Palaeoecol.*, *309*(1–2), 98–110.

Dowsett, H., R. Thompson, J. Barron, T. Cronin, F. Fleming, S. Ishman, R. Poore, D. Willard, and T. Holtz (1994), Joint investigations of the middle pliocene climate. 1. PRISM paleoenvironmental reconstructions, *Global Planet. Change*, *9*(3–4), 169–195.

Dowsett, H., M. Robinson, A. Haywood, U. Salzmann, D. Hill, L. Sohl, M. Chandler, M. Williams, K. Foley, and D. Stoll (2010), The PRISM3D paleoenvironmental reconstruction, *Stratigraphy*, *7*(2–3), 123–139.

Dowsett, H. J., et al. (2013), Sea surface temperature of the mid-Piacenzian ocean: A data-model comparison, *Sci. Rep.*, *3*, 2013, doi:10.1038/srep02013.

Edwards, J. M., and A. Slingo (1996), Studies with a flexible new radiation code. 1. Choosing a configuration for a large-scale model, *Q. J. R. Meteorol. Soc.*, *122*(531), 689–719.

Fairbanks, R., M. Evans, J. Rubenstone, R. Mortlock, K. Broad, M. Moore, and C. Charles (1997), Evaluating climate indices and their geochemical proxies measured in corals, *Coral Reefs*, *16*, S93–S100, doi:10.1007/s003380050245.

Gordon, C., C. Cooper, C. Senior, H. Banks, J. Gregory, T. Johns, J. Mitchell, and R. Wood (2000), The simulation of SST, sea ice extents and ocean heat transports in a version of the Hadley Centre coupled model without flux adjustments, *Clim. Dyn.*, *16*(2–3), 147–168.

Gregory, D., and D. Morris (1996), The sensitivity of climate simulations to the specification of mixed phase clouds, *Clim. Dyn.*, *12*(9), 641–651.

Gregory, D., and P. R. Rowntree (1990), A mass flux convection scheme with representation of cloud ensemble characteristics and stability-dependent closure, *Mon. Weather Rev.*, *118*(7), 1483–1506.

Haywood, A. M., P. J. Valdes, and B. W. Sellwood (2000), Global scale palaeoclimate reconstruction of the middle Pliocene climate using the UKMO GCM: Initial results, *Global Planet. Change*, *25*(3–4), 239–256.

Haywood, A. M., et al. (2010), Pliocene Model Intercomparison Project (PlioMIP): Experimental design and boundary conditions (Experiment 1), *Geosci. Model Dev.*, *3*(1), 227–242.

Haywood, A. M., H. J. Dowsett, M. M. Robinson, D. K. Stoll, A. M. Dolan, D. J. Lunt, B. Otto-Bliesner, and M. A. Chandler (2011), Pliocene Model Intercomparison Project (PlioMIP): Experimental design and boundary conditions (Experiment 2), *Geosci. Model Dev.*, *4*(3), 571–577.

Haywood, A. M., et al. (2013a), Large-scale features of Pliocene climate: Results from the Pliocene Model Intercomparison Project, *Clim. Past*, *9*(1), 191–209.

Haywood, A. M., et al. (2013b), On the identification of a Pliocene time slice for data-model comparison, *Philos. Trans. R. Soc. A*, *371*(2001), 20120515, doi:10.1098/rsta.2012.0515.
Hewitt, H. T., D. Copsey, I. Culverwell, C. Harris, R. S. R. Hill, A. B. Keen, A. J. McLaren, and E. C. Hunke (2011), Design and implementation of the infrastructure of HadGEM3: The next-generation Met Office climate modelling system, *Geosci. Model Dev.*, *4*(2), 223–253.
Hill, D. J., A. Z. Csank, A. M. Dolan, and D. J. Lunt (2011), Pliocene climate variability: Northern Annular Mode in models and tree-ring data, *Palaeogeogr. Palaeoclimatol. Palaeoecol.*, *309*(1–2), 118–127.
Hoffmann, G., J. Jouzel, and V. Masson (2000), Stable water isotopes in atmospheric general circulation models, *Hydrol. Process.*, *14*(8), 1385–1406.
Ivanovic, R. F., P. J. Valdes, R. Flecker, L. J. Gregoire, and M. Gutjahr (2013), The parameterisation of Mediterranean-Atlantic water exchange in the Hadley Centre model HadCM3, and its effect on modelled North Atlantic climate, *Ocean Modell.*, *62*, 11–16.
Jones, D. S., and W. D. Allmon (1995), Records of upwelling, seasonality and growth in stable-isotope profiles of Pliocene mollusk shells from Florida, *Lethaia*, *28*(1), 61–74.
Joussaume, S., R. Sadourny, and J. Jouzel (1984), A general-circulation model of water isotope cycles in the atmosphere, *Nature*, *311*(5981), 24–29.
Jouzel, J., G. Hoffmann, R. D. Koster, and V. Masson (2000), Water isotopes in precipitation: Data/model comparison for present-day and past climates, *Quat. Sci. Rev.*, *19*(1–5), 363–379.
Kaplan, J. O. (2001), Geophysical applications of vegetation modeling, PhD thesis, Lund Univ., Lund, Sweden.
Karas, C., D. Nurnberg, R. Tiedemann, and D. Garbe-Schonberg (2011), Pliocene climate change of the Southwest Pacific and the impact of ocean gateways, *Earth Planet. Sci. Lett.*, *301*(1–2), 117–124.
Karas, C., D. Nuernberg, A. K. Gupta, R. Tiedemann, K. Mohan, and T. Bickert (2009), Mid-Pliocene climate change amplified by a switch in Indonesian subsurface throughflow, *Nat. Geosci.*, *2*(6), 433–437, doi:10.1038/NGEO520.
Lee, J.-E., I. Fung, D. J. DePaolo, and C. C. Henning (2007), Analysis of the global distribution of water isotopes using the NCAR atmospheric general circulation model, *J. Geophys. Res.*, *112*, D16306, doi:10.1029/2006JD007657.
Lee, J.-E., K. Johnson, and I. Fung (2009), Precipitation over South America during the Last Glacial Maximum: An analysis of the "amount effect" with a water isotope-enabled general circulation model, *Geophys. Res. Lett.*, *36*, L19701, doi:10.1029/2009GL039265.
Lee, J.-E., C. Risi, I. Fung, J. Worden, R. A. Scheepmaker, B. Lintner, and C. Frankenberg (2012), Asian monsoon hydrometeorology from TES and SCIAMACHY water vapor isotope measurements and LMDZ simulations: Implications for speleothem climate record interpretation, *J. Geophys. Res.*, *117*, D15112, doi:10.1029/2011JD017133.
LeGrande, A., and G. Schmidt (2006), Global gridded data set of the oxygen isotopic composition in seawater, *Geophys. Res. Lett.*, *33*, L12604, doi:10.1029/2006GL026011.
LeGrande, A. N., and G. A. Schmidt (2011), Water isotopologues as a quantitative paleosalinity proxy, *Paleoceanography*, *26*, PA3225, doi:10.1029/2010PA002043.
Mathieu, R., D. Pollard, J. Cole, J. White, R. Webb, and S. Thompson (2002), Simulation of stable water isotope variations by the GENESIS GCM for modern conditions, *J. Geophys. Res.*, *107*(D4), ACL 2–1–ACL 2-18, doi:10.1029/2001JD900255.
Miller, K. G., J. D. Wright, J. V. Browning, A. Kulpecz, M. Kominz, T. R. Naish, B. S. Cramer, Y. Rosenthal, W. R. Peltier, and S. Sosdian (2012), High tide of the warm Pliocene: Implications of global sea level for Antarctic deglaciation, *Geology*, *40*(5), 407–410.
Noone, D., and I. Simmonds (2002), Associations between delta O-18 of water and climate parameters in a simulation of atmospheric circulation for 1979–95, *J. Clim.*, *15*(22), 3150–169.
Pope, V., M. Gallani, P. Rowntree, and R. Stratton (2000), The impact of new physical parametrizations in the Hadley Centre climate model: HadAM3, *Clim. Dyn.*, *16*(2–3), 123–146.
Pound, M. J., J. Tindall, S. J. Pickering, A. M. Haywood, H. J. Dowsett, and U. Salzmann (2014), Late Pliocene lakes and soils: A global data set for the analysis of climate feedbacks in a warmer world, *Clim. Past*, *10*(1), 167–180, doi:10.5194/cp-10-167-2014.
Prescott, C. L., A. M. Haywood, A. M. Dolan, S. J. Hunter, J. O. Pope, and S. J. Pickering (2014), Assessing orbitally-forced interglacial climate variability during the mid-Pliocene Warm Period, *Earth Planet. Sci. Lett.*, *400*, 261–271.
Risi, C., S. Bony, F. Vimeux, and J. Jouzel (2010), Water-stable isotopes in the LMDZ4 general circulation model: Model evaluation for present-day and past climates and applications to climatic interpretations of tropical isotopic records, *J. Geophys. Res.*, *115*, D12118, doi:10.1029/2009JD013255.
Roberts, C. D., A. N. LeGrande, and A. K. Tripati (2011), Sensitivity of seawater oxygen isotopes to climatic and tectonic boundary conditions in an early Paleogene simulation with GISS ModelE-R, *Paleoceanography*, *26*, PA4203, doi:10.1029/2010PA002025.
Roden, J. S., G. G. Lin, and J. R. Ehleringer (2000), A mechanistic model for interpretation of hydrogen and oxygen isotope ratios in tree-ring cellulose, *Geochim. Cosmochim. Acta*, *64*(1), 21–35.
Rohling, E. J. (2007), Progress in paleosalinity: Overview and presentation of a new approach, *Paleoceanography*, *22*, PA3215, doi:10.1029/2007PA001437.
Rostek, F., G. Ruhland, F. Bassinot, P. Muller, L. Labeyrie, Y. Lancelot, and E. Bard (1993), Reconstructing sea-surface temperature and salinity using delta-O-18 and alkenone records, *Nature*, *364*(6435), 319–321, doi:10.1038/364319a0.
Russon, T., A. W. Tudhope, G. C. Hegerl, M. Collins, and J. Tindall (2013), Inter-annual tropical Pacific climate variability in an isotope-enabled CGCM: Implications for interpreting coral stable oxygen isotope records of ENSO, *Clim. Past*, *9*(4), 1543–1557, doi:10.5194/cp-9-1543-2013.
Salzmann, U., et al. (2013), Challenges in quantifying Pliocene terrestrial warming revealed by data-model discord, *Nat. Clim. Change*, *3*(11), 969–974.
Schmidt, G. A., A. N. Legrande, and G. Hoffmann (2007), Water isotope expressions of intrinsic and forced variability in a coupled ocean-atmosphere model, *J. Geophys. Res.*, *112*, D10103, doi:10.1029/2006JD007781.
Semtner, A. J. (1976), Model for thermodynamic growth of sea ice in numerical investigations of climate, *J. Phys. Oceanogr.*, *6*(3), 379–389.
Sime, L. C., C. Risi, J. C. Tindall, J. Sjolte, E. W. Wolff, V. Masson-Delmotte, and E. Capron (2013), Warm climate isotopic simulations: What do we learn about interglacial signals in Greenland ice cores?, *Quat. Sci. Rev.*, *67*, 59–80.
Smith, R. N. B. (1990), A scheme for predicting layer clouds and their water-content in a general-circulation model, *Q. J. R. Meteorol. Soc.*, *116*(492), 435–460.
Snelling, A. M., G. E. A. Swann, J. Pike, and M. J. Leng (2014), Pliocene diatom and sponge spicule oxygen isotope ratios from the Bering Sea: Isotopic offsets and future directions, *Clim. Past*, *10*(5), 1837–1842, doi:10.5194/cp-10-1837-2014.
Solomon, S., D. Qin, M. Manning, A. M. M. Z. Chen, K. B. Averyt, M. Tignor, and H. L. Miller (Eds.) (2007), *IPCC, 2007 Climate Change 2007: The Physical Science Basis. Contribution of Working Group I to the Fourth Assessment Report of the Intergovernmental Panel on Climate Change*, Cambridge Univ. Press, Cambridge, U. K., and New York.

Stocker, T. F., D. Qin, G. K. Plattner, M. Tignor, S. K. Allen, J. Boschung, A. Nauels, Y. Xia, V. Bex, and P. M. Midgley (Eds.) (2013), *IPCC, 2013 Climate Change 2013: The Physical Science Basis. Contribution of Working Group I to the Fifth Assessment Report of the Intergovernmental Panel on Climate Change*, Cambridge Univ. Press, Cambridge, U. K., and New York.

Tian, J., P. Wang, X. Cheng, and Q. Li (2002), Astronomically tuned Plio-Pleistocene benthic delta O-18 record from South China Sea and Atlantic-Pacific comparison, *Earth Planet. Sci. Lett.*, *203*(3–4), 1015–1029, doi:10.1016/S0012-821X(02)00923-8.

Tindall, J., R. Flecker, P. Valdes, D. N. Schmidt, P. Markwick, and J. Harris (2010), Modelling the oxygen isotope distribution of ancient seawater using a coupled ocean-atmosphere GCM: Implications for reconstructing early Eocene climate, *Earth Planet. Sci. Lett.*, *292*(3–4), 265–273, doi:10.1016/j.epsl.2009.12.049.

Tindall, J. C., and P. J. Valdes (2011), Modeling the 8.2 ka event using a coupled atmosphere-ocean GCM, *Global Planet. Change*, *79*(3–4), 312–321, doi:10.1016/j.gloplacha.2011.02.004.

Tindall, J. C., P. J. Valdes, and L. C. Sime (2009), Stable water isotopes in HadCM3: Isotopic signature of El Nino Southern Oscillation and the tropical amount effect, *J. Geophys. Res.*, *114*, D04111, doi:10.1029/2008JD010825.

Vaks, A., J. Woodhead, M. Bar-Matthews, A. Ayalon, R. A. Cliff, T. Zilberman, A. Matthews, and A. Frumkin (2013), Pliocene-Pleistocene climate of the northern margin of Saharan-Arabian Desert recorded in speleothems from the Negev Desert, Israel, *Earth Planet. Sci. Lett.*, *368*, 88–100, doi:10.1016/j.epsl.2013.02.027.

Vuille, M., R. Bradley, R. Healy, M. Werner, D. Hardy, L. Thompson, and F. Keimig (2003), Modeling delta O-18 in precipitation over the tropical Americas: 2. Simulation of the stable isotope signal in Andean ice cores, *J. Geophys. Res.*, *108*(D6), 4175, doi:10.1029/2001JD002039.

Wara, M. W., A. C. Ravelo, and M. L. Delaney (2005), Permanent El Nino-like conditions during the Pliocene warm period, *Science*, *309*(5735), 758–761.

Watanabe, T., et al. (2011), Permanent El Nino during the Pliocene warm period not supported by coral evidence, *Nature*, *471*(7337), 209–211.

Werner, M., P. M. Langebroek, T. Carlsen, M. Herold, and G. Lohmann (2011), Stable water isotopes in the ECHAM5 general circulation model: Toward high-resolution isotope modeling on a global scale, *J. Geophys. Res.*, *116*, D15109, doi:10.1029/2011JD015681.

Williams, M., A. M. Haywood, E. M. Harper, A. L. A. Johnson, T. Knowles, M. J. Leng, D. J. Lunt, B. Okamura, P. D. Taylor, and J. Zalasiewicz (2009), Pliocene climate and seasonality in North Atlantic shelf seas, *Philos. Trans. R. Soc. A*, *367*(1886), 85–108.

Williams, M., A. Haywood, C. Hillenbrand, and I. Wilkinson (2005), Efficacy of delta O-18 data from Pliocene planktonic foraminifer calcite for spatial sea surface temperature reconstruction: Comparison with a fully coupled ocean-atmosphere GCM and fossil assemblage data for the mid-Pliocene, *Geol. Mag.*, *142*(4), 399–417, doi:10.1017/S0016756805000828.

Winnick, M. J., J. M. Welker, and C. P. Chamberlain (2013), Stable isotopic evidence of El Nino-like atmospheric circulation in the Pliocene western United States, *Clim. Past*, *9*(5), 2085–2099.

Zhang, R., et al. (2013), Mid-Pliocene East Asian monsoon climate simulated in the PlioMIP, *Clim. Past*, *9*(9), 903–912.

Zhou, J., C. J. Poulsen, D. Pollard, and T. S. White (2008), Simulation of modern and middle Cretaceous marine delta O-18 with an ocean-atmosphere general circulation model, *Paleoceanography*, *23*, PA3223, doi:10.1029/2008PA001596.